Available online at www.sciencedirect.com
SCIENCE DIRECT®
Journal of the European Ceramic Society 25 (2005) 3427–3435
www.elsevier.com/locate/jeurceramsoc

The use of image analysis for sintering investigations: The example of CeO_2 doped with TiO_2

M. Coster[a], X. Arnould[a], J.L. Chermant[b], L. Chermant[b], T. Chartier[c,*]

[a] *UFR Sciences and SIFCOM, UMR CNRS 6176, 6 Bd du Maréchal Juin, 14050 Caen, Cedex, France*
[b] *LARMAUR, FRE CNRS 2717, Bât 10B, Université de Rennes 1, Campus de Beaulieu, F-35042 Rennes, Cedex, France*
[c] *SPCTS, UMR CNRS 6638, Ecole Nationale Supérieure de Céramique Industrielle, 47-73 Avenue Albert Thomas, F-87065 Limoges, Cedex, France*

Received 10 June 2004; received in revised form 31 August 2004; accepted 5 September 2004
Available online 28 October 2004

Abstract

This paper deals with the use of automatic image analysis to provide access to the morphological parameters of the microstructure during the sintering of ceria. Some specific techniques of image processing have been required and performed to automatically measure the change in the specific surface area, the integral of mean curvature per unit volume, the contiguity and the grain size distribution. The diffusional paths, the kinetics of densification and the mobility of the grain boundaries were determined. A value of about 2 was obtained for the grain size exponent. The densification at 1300 °C and probably at 1200 °C is governed by the volume diffusion of the slowest species. Moreover, the use of a TiO_2 dopant makes it possible to control the migration of the CeO_2 grain boundaries and thus to limit grain growth.

Keywords: Image analysis; CeO_2; Microstructure; Sintering

1. Introduction

Controlling densification and grain growth, which both occur during sintering, is a critical issue for the processing and the application of advanced ceramics. Dense, fine and homogeneous microstructures are generally desirable for structural parts. Then, the understanding of mass-transport mechanisms during sintering is necessary to control the reliability and the properties of the final parts.

Many sintering models of densification and of grain growth in polycrystalline materials have been developed,[1–6] generally based on diffusional transport of matter due to differential surface curvature of grain surfaces. Using these models to determine the mechanism of transport, which depends on the diffusional paths, requires a correct quantitative description of the evolution of the pertinent parameters of the microstructure (morphological parameters) under controlled conditions (temperature, time, atmosphere, ...) during the thermal treatment.

There has been a considerable work performed on measuring grain size and size distribution but rather less on the use of stereological parameters,[7–9] such as specific surface area per unit volume or mean curvature of pores and grains. Today, these parameters can be estimated easily if automatic methods of image processing and mathematical morphology are utilized.[10,11] The mathematical morphology makes it possible to characterize the phases and grains of a microstructure. Furthermore, the treatment speed makes it possible to analyze many images. So the conditions for a good statistical analysis are always verified and the degree of microstructural homogeneity can also be evaluated. Moreover, the evolution of such morphological parameters leads to a knowledge of the sintering mechanism, which can be compared to the information given by dilatometry investigations.[9,11,12]

CeO_2 doped with TiO_2, with relatively homogeneous microstructure and moderate grain growth, has been chosen as an interesting model system to study the sintering

* Corresponding author. Tel.: +33 5 5545 2222; fax: +33 5 5579 0998.
E-mail address: t.chartier@ensci.fr (T. Chartier).

0955-2219/$ – see front matter © 2004 Elsevier Ltd. All rights reserved.
doi:10.1016/j.jeurceramsoc.2004.09.003

both by classical methods[13] and by image analysis.[14] CeO_2 based ceramics are of interest as materials for catalyst supports, as ionic conductors for solid electrolyte and as gas sensors.[15–17] Other applications of CeO_2 are as host material for radioactive actinides[18] or as nanocrystalline thin films for optoelectronics.[19]

The present paper is devoted to the study of the sintering of CeO_2 doped with TiO_2, using morphological parameters determined by image analysis. It is based on the thesis of Arnould.[14]

2. Experimental

2.1. Sample preparation

A 99.95% pure commercial CeO_2 powder (Opaline grade, Rhône-Poulenc, France) with a mean particle size of 0.7 μm and a specific surface area of 2.7 $m^2\,g^{-1}$ was used. The CeO_2 powder was first deagglomerated by attrition milling for 30 min in 2-propanol with zirconia balls. An amount of titanium butoxide ($Ti[O(CH_2)_3CH_3]_4$, Aldrich, France), corresponding to 0.1 wt.% of TiO_2 with respect to CeO_2, was added in the attrition bowl. A subsequent milling of 15 min was performed. Then, the titanium butoxide was hydrolyzed by the addition of 15 mol of water for 1 mol of titanium butoxide with an additional milling of 15 min. Polyethylene glycol 1500 (3 wt.% on the basis of dry powder), was added in order to confer the cohesion of the pressed green parts. After evaporation of the solvent, the dry powder was granulated by using a 315 μm sieve.

Cylinders (20 mm in diameter, 5 mm thick) were obtained by dry pressing the granulated powder under 150 MPa. Then the organic additives were removed by pyrolysis at 500 °C for 3 h in air. The resulting samples were sintered with a rapid heating rate of 20 °C min^{-1} up to the sintering temperature (1100, 1200, 1300, 1400 or 1450 °C). After the dwell (6, 18, 36, 60, 120, 300, 600 or 1200 min), specimens were fast cooled at 50 °C min^{-1}. The density was measured by the Archimedes technique in distilled water.

The samples were polished with progressing finer grades of diamond paste until the 0.25 μm grade. Grain boundaries were revealed by thermal etching for 5 min at a temperature 50 °C lower than the sintering temperature.

2.2. Image processing and image analysis

Before making measurements on the microstructure, it is necessary to perform a treatment of images to correctly distinguish grain boundaries and porosity. For all materials, the images of pores are obtained by using an automatic threshold.

A morphological treatment was designed for materials with a relative density higher than 63% as described in Arnould and coworkers[14,20,21]

Two methods, depending on the porosity, were developed. For materials with a relative density larger than 85%, the images of pores were first obtained. Then, the images of grain boundaries were extracted by a top-hat transformation fol-

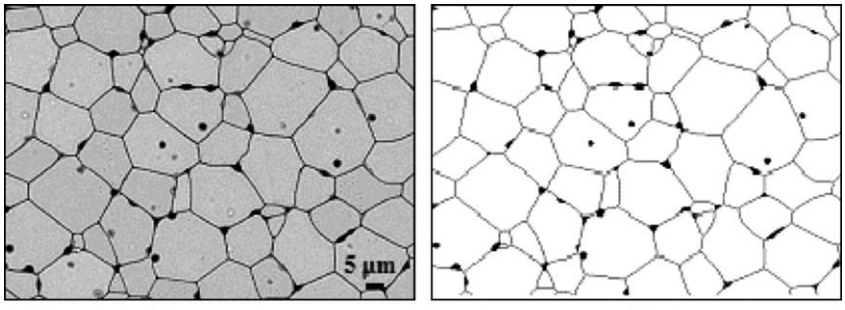

Fig. 1. (a) Initial image (CeO_2 sintered at 1300 °C, during 20 h); (b) final binary image.

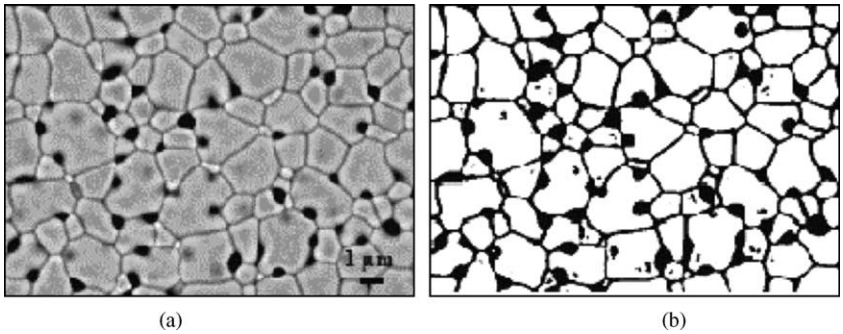

Fig. 2. (a) Initial image (CeO_2 sintered at 1300 °C, during 36 min); (b) final binary image.

lowed by a thinning.[10] The obtained images still need an additional treatment to eliminate the artifacts due to over- and/or under-segmentation. Fig. 1 illustrates the corresponding image sequence.

For materials with a relative density ranging from 63 to 85%, images are of less good quality and require a more complex morphological treatment. This treatment involves a linear filtering to decrease noise. Grain boundaries are then enhanced by a morphological gradient filter followed by a threshold.[10,11] Finally, segmentation by watershed on the gradient image was performed from the markers of grains selected according to an area criterion.[10,11] Fig. 2 illustrates the corresponding image sequence.

This image treatment makes it possible to determine the nature of porosity (intra- or inter-granular) and the two specific types of surface, namely the solid/pore interface, S_V(S/P), and the solid/solid interface comprising the grain boundaries, S_V(S/S). The stereological methods are detailed in Appendix A.

3. Morphological study of sintering

3.1. Study of the homogeneity

One of the merits of image analysis in material sciences is its statistical character. To obtain significant measurements, it is necessary to make sure that sampling corresponds to a sufficiently homogeneous zone. In order to investigate the homogeneity of a microstructure on some samples, a geostatistic tool is utilized, namely, the regularized variogram[22] (see also Chapter IX in Serra[10]). If $f(x)$ is an average measure on a field of analysis set in x, and $f(x+h)$ the same measure in $x+h$, the regularized variogram is defined as the mathematical expectation of the quadratic distance between these measures:

$$\gamma(h) = \tfrac{1}{2}E[(f(x) - f(x+h))^2] \quad (1)$$

If homogeneity is reached, a plateau of the variogram is observed. In our case $f(x)$ is either the connectivity number (number of grains) by unity of surface area, N_A(G), or the volume fraction of the porous phase, V_V(P). The variogram corresponding to the connectivity number quickly reaches a constant value (up to the statistical fluctuations) (Fig. 3). This result is always verified whatever the set of fields of measurements: on the edge or in the bulk of the sample. Then, the material microstructure can be considered as homogeneous. It is not the case if measurements concern the fraction of the porous phase on the edge of the samples (Fig. 4). Only the bulk is homogeneous. According to these results, only the bulk part of samples will be analyzed for the following investigation. Finally, to verify the isotropy of the microstructure, the measurement of the number of grains per unit length, N_L(G,α), according to the orientation α, was undertaken.

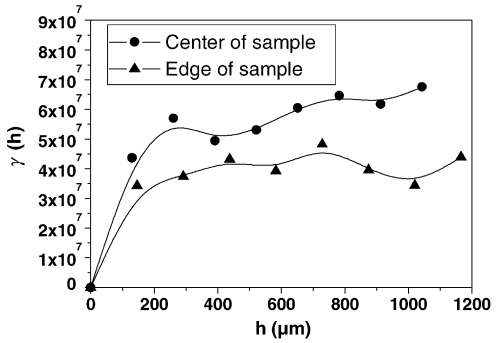

Fig. 3. Variogram of the connectivity number of CeO_2 grains, for a material sintered at 1300 °C during 5 h.

3.2. Evolution of morphological parameters during sintering

3.2.1. Evolution according to volume fraction of ceria

The strategy of sampling being chosen, some morphological parameters were selected to follow the evolution of the microstructure. From a practical point of view, this microstructure cannot be revealed, nor segmented, before a certain degree of densification, i.e. 63% of theoretical density, has been reached. So, the parameters, which can be followed during all the stages of densification, must be distinguished from those accessible only on segmented images.

Stereological parameters always accessible are the content of the phase CeO_2, i.e. the volume fraction of the solid phase, V_V(S), the specific surface area between the ceria and the pores, S_V(S/P), and the integral of mean curvature by unity of volume, M_V(S/P). We know that V_V(S) is the indicator of the densification and constitutes the variable which makes it possible to follow the other parameters. The change in S_V(S/P) as a function of V_V(S) is roughly monotonous in its decrease and does not require any comment (Fig. 5). According to the definition of M_V(S/P), M_V(S/P) shows negative values because pores behave as holes in the material (Fig. 6) (see Chapter V in Serra[10]). These values increase to reach the zero value of the dense material. However, decreases observed between 30 and 37% of porosity correspond to the formation of isolated pores associated to the closure of chan-

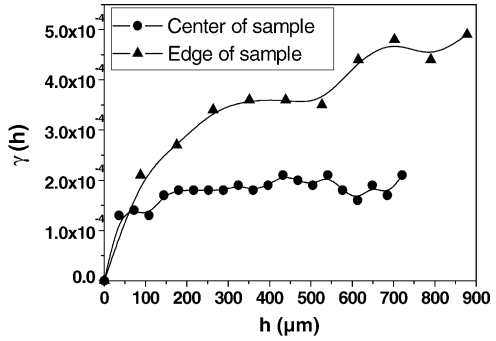

Fig. 4. Variogram of the porosity for CeO_2 sintered at 1300 °C during 36 min.

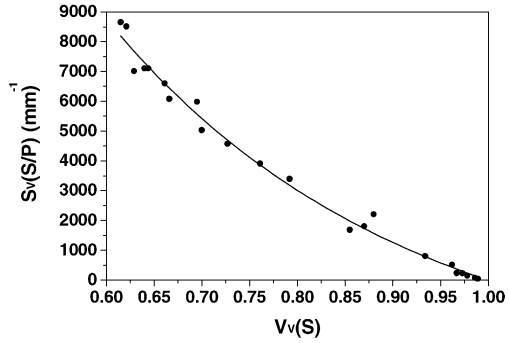

Fig. 5. Evolution of S_V(S/P), as a function of the volume fraction of CeO_2, V_V(S).

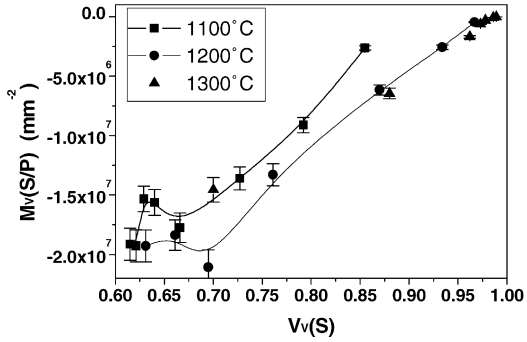

Fig. 6. Evolution of M_V(S/P), as a function of the volume fraction of CeO_2, V_V(S).

nels. This makes it possible to know exactly at what stage of sintering isolated pores begin to appear.

Thanks to the image segmentation techniques and the fact that all grain boundaries are revealed, it is possible to follow the evolution of other pertinent stereological parameters such as the total specific surface area, S_V(S/S + S/P), (Fig. 7), and a derived parameter, the contiguity of the polycrystalline phase, C(S/S), (Fig. 8), defined as:

$$C(\mathrm{S/S}) = \frac{2S_V(\mathrm{S/S})}{2S_V(\mathrm{S/S}) + S_V(\mathrm{S/P})} \quad (2)$$

The evolution of these two parameters shows a very different behavior for the specimens sintered at 1200 °C and for

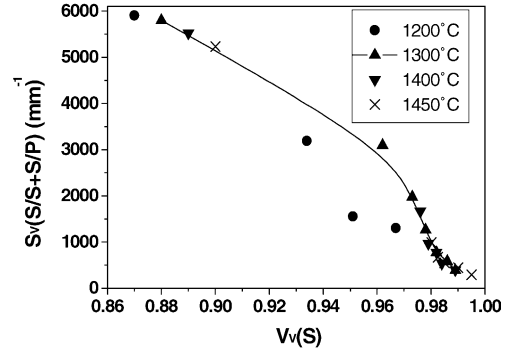

Fig. 7. Evolution of the total specific surface area, S_V(S/S + S/P), as a function of the volume fraction of ceria, V_V(S).

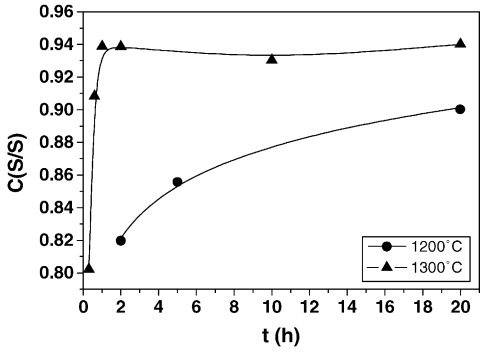

Fig. 8. Evolution of the parameter of contiguity, C(S/S), as a function of the sintering time, t.

those sintered at and above 1300 °C. Finally, the reconstruction of the grains boundaries makes it possible to reach the 2D granulometry of the ceria and particularly its mean grain size.

3.2.2. Evolution according to time and temperature

When segmentation is possible (density higher than 63 wt.%), it gives access to the total specific area S_V(S/S + S/P) and to the total mean curvature M_V(S/S + S/P). So the change of these parameters as a function of time and temperature was studied. Assuming that we are only in the presence of a scale effect, DeHoff[23] has shown that stereological parameters follow a law of the type:

$$W^{m/d}(X) - W_0^{m/d}(X) = kt \quad (3)$$

where m is the kinetics exponent and the low exponent d the scaling of the stereological parameter W($d = -1$ for S_V and $d = -2$ for M_V). For these two parameters, expression (3) gives:

$$S_V^{-m}(X) - S_{V_0}^{-m}(X) = kt \quad \text{and}$$
$$M_V^{-m/2}(X) - M_{V_0}^{-m/2}(X) = kt \quad (4)$$

The best agreement between the experimental results and those theoretical laws is obtained for a value of m equal to 2 for all samples. From these results, the activation energy of the evolution of total specific area and of the total mean curvature can be calculated from the following expression:

$$W(X) - W_0(X) = k_0 \left[\exp\left(-\frac{E_A}{RT}\right)\right]^m t^m \quad (5)$$

The activation energy determined from S_V and from M_V ranges between 390 and 415 kJ mol^{-1}. No values for comparison have been found in the literature.

3.3. Kinetics of densification

As the transport of species during sintering can be governed by various mechanisms, which depend on diffusion path and particularly on the character of the grain

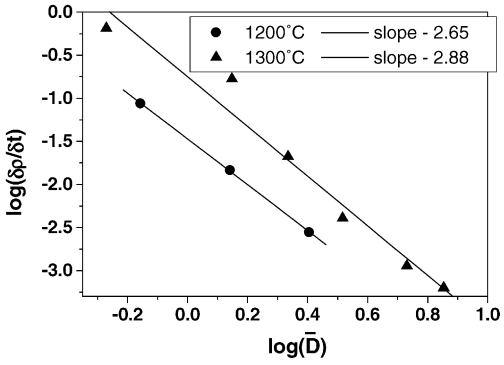

Fig. 9. Rate of densification, $\delta\rho/\delta t$, as a function of $\bar{D}$ at 1200 and 1300 °C.

boundaries,[1–6] it is absolutely necessary to use segmented images to estimate the grain size. The densification rate can be written as a function of the temperature, T, the mean grain size, $\bar{D}$, obtained from individual analysis on segmented images, and a variable A which depends also on the average coefficient of diffusion (in the case of several simultaneous mechanisms):[24]

$$\frac{\partial\rho}{\partial t} = \frac{\partial(1 - V_V(P))}{\partial t} = \frac{A}{T\bar{D}^n} \quad (6)$$

In this relationship, the exponent n is characteristic of the limiting mechanism of transport, which governs the kinetics of densification. Then, the exponent n, which depends on the path of diffusion, is equal to 3 in the case of diffusion in the volume and to 4 for diffusion at grain boundaries. The estimation of the derivative is made by approximation of the curve $(1 - V_V(P)) = f(t)$ by a polynomial equation of order 2.

Considering the fast densification at high temperature, the kinetics of densification was only investigated at 1200 and 1300 °C (Fig. 9). For a temperature of 1300 °C, a slope close to −3 (−2.88) was obtained with a good correlation. This suggests that the limiting mechanism is diffusion in the volume. For 1200 °C, the agreement is less good (−2.65), but only three experimental points are available and it is difficult to give a final conclusion.

From the complete relationships of the rate of densification given by Coble,[2] one can extract the coefficient of diffusion in volume of the slowest element:

$$\frac{\partial\rho}{\partial t} = \frac{355 D_V \tau \Omega}{RT\bar{D}^3} \quad (7)$$

where D_V is the diffusion coefficient in the volume, τ is the surface energy, Ω is the molar volume, and R is the gas constant.

Calculation was made using the following numerical values:

- $\tau = 1\ \mathrm{J\,m^{-2}}$ a typical value for the surface energy of oxides, (see for example[25])
- $\Omega = 23.69\ \mathrm{cm^3\,mol^{-1}}$.

Table 1
Values of the parameters n and k for the kinetics laws of grain growth (Eq. (3)) of CeO_2, for various temperatures of sintering

Temperature (°C)	n	k
1200	2.2	0.73
1300	1.9	3.81
1400	2.0	20.05
1450	2.1	45.91

Assuming that the densification takes place by diffusion in the volume both at 1200 and 1300 °C, the coefficients of diffusion obtained at 1200 and 1300 °C are, respectively, 1.6×10^{-13} and $7.9 \times 10^{-13}\ \mathrm{cm^2\,s^{-1}}$. These calculated values are of the same order of magnitude as the values determined for yttrium oxide.[25]

3.4. Kinetics of grain growth

The evolution of the average diameter of grains as a function of time, for various temperatures, was determined with precision by image analysis. Laws comparable to that of DeHoff (Eq. (3)) were found.[23] The n exponent is close to 2 whatever the temperature (Table 1). At 1200 °C, only four points are available and correct coefficients of correlation were obtained for both $m = 3$ (0.97) and $m = 2$ (0.99). Then, one cannot affirm that the mechanism of grain growth is identical at 1200 °C and above 1300 °C. Some values of the n exponent, reported in the literature,[26–30] obtained for various types of doped CeO_2 are given in Table 2. The results vary from one author to another, for the same system (pure CeO_2). The adaptation of experimental results, with power laws, is always a problem because there is a lot of uncertainty in the estimation of n.

By referring to the data given by Brook,[31] the mechanism which limits grain growth, would appear to be grain boundary pinning by the segregation of inclusions at grain boundaries.

The inclusions control the migration of the grain boundaries. According to the literature,[13,32] only one defined compound, i.e. $CeTi_2O_6$, is known in the CeO_2–TiO_2 system, in oxidizing conditions in air. Guka and Kolar reported that the temperature of formation of $CeTi_2O_6$ is about 1270 °C and its non-congruent melting temperature is 1365 °C.[32] The presence of inter- and intra-granular inclusions of $CeTi_2O_6$ in CeO_2 materials sintered at a temperature up to 1300 °C was verified by scanning electron microscopy (Fig. 10).

Table 2
Values of the n exponent for the kinetics law of CeO_2 grain growth

Reference	Material	Temperature (°C)	Exponent n
Chen[26]	CeO_2 pure	1270–1420	2
Zhang[27]	CeO_2 pure	1350–1500	3
	CeO_2 + 1% Mn	1350–1500	4
Zhang[28]	CeO_2 + 0.5% Fe	1350–1500	4
Zhang[29]	CeO_2 + 0.25% Co	1350–1500	4
Ji-Guang[30]	CeO_2 + (5–20)% Sm	1100–1400	2

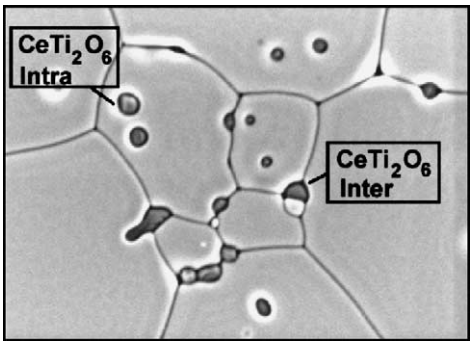

Fig. 10. SEM image of a sample CeO_2 elaborated at 1300 °C during 20 h, showing the presence of the $CeTi_2O_6$ inclusions in inter- and intra-granular position.

In the case of grain-boundary pinning by second phase particles, the mobility M of the grain boundaries can be estimated from the kinetic law of growth:[33,34]

$$\frac{\partial \bar{D}}{\partial t} = \frac{M\gamma}{\bar{D}} - f(\bar{D}) \tag{8}$$

where γ is the energy of the grain boundary, a value considered constant and estimated as 0.3 J m^{-2} and $f(\bar{D})$ represents the drag influence on the growth rate caused by boundary pinning. With the reasonable assumption that $\bar{D}$ can approach a maximum size $\bar{D}_{max}$ for a second phase inclusions, that is in agreement with Fig. 11, the drag term $f(\bar{D})$ in Eq. (8) becomes independent of the main grain size $\bar{D}$ and Eq. (8) can be rewritten as:

$$\frac{\partial \bar{D}}{\partial t} = M\gamma\left(\frac{1}{\bar{D}} - \frac{1}{\bar{D}_{max}}\right) \tag{9}$$

That leads to a parabolic law:

$$\frac{M\gamma}{D_{max}^2}t = \frac{\bar{D}_0 - \bar{D}}{D_{max}} + \ln\left(\frac{\bar{D}_{max} - \bar{D}_0}{\bar{D}_{max} - \bar{D}}\right) \tag{10}$$

where $\bar{D}_0$ is the initial mean grain size.

Calculated values of mobility are compared to values reported by Chen et al.[26] in Table 3. Our results follow the same evolution with temperature and are of the same order of magnitude.

Table 3
Mobility of grain boundaries of CeO_2, with addition of TiO_2, for various temperatures of sintering

Temperature (°C)	Mobility of grain boundaries (10^{-16} m^3/Ns)		
	This work	Chen[26]	
	$[Ti^{4+}] \cong 0.2$ at.%	$[Ti^{4+}] = 0.1$ at.%	$[Ti^{4+}] = 1$ at.%
1200	3		
1270		48	4.2
1300	18		
1320		140	14
1370		365	37
1400	93		
1420		1018	97
1450	212		

Table 4
Activation energy of grain boundary mobility for pure CeO_2 and doped CeO_2

Reference	Material	Activation energy of grain boundary mobility (kJ mol^{-1})
This work	CeO_2 + 0.2% Ti^{4+}	350
Chen[26]	Pure CeO_2	581
	CeO_2 + 0.1% Ti^{4+}	438
	CeO_2 + 1% Ti^{4+}	453
Zhang[27]	Pure CeO_2	731
	CeO_2 + 1% Mn	593
Zhang[28]	Pure CeO_2	731
	CeO_2 + 0.5% Fe	590
Zhang[29]	Pure CeO_2	697
	CeO_2 + 0.25% Co	572
Ji-Guang[30]	CeO_2 + (5–20)% Sm	254

This mobility follows the Arrhenius law, making it possible to calculate an activation energy of 350 kJ mol^{-1}, which is compared to values from the literature (Table 4).

The knowledge of the mean grain size of ceria (Fig. 11) and porosity makes it possible to draw the sintering trajectories (i.e. mean grain size versus density) (Fig. 12). The densification is the most important mechanism at the beginning of sintering. Grain growth remains very low, for a density

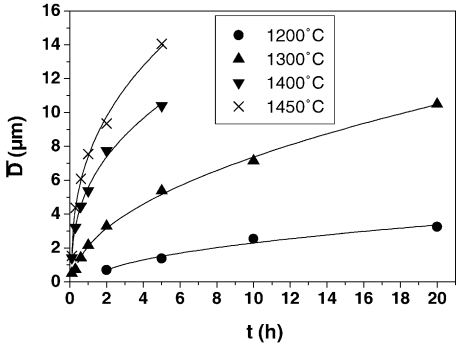

Fig. 11. Evolution of mean grain size of ceria, $\bar{D}$, as a function of time, t, for different temperatures.

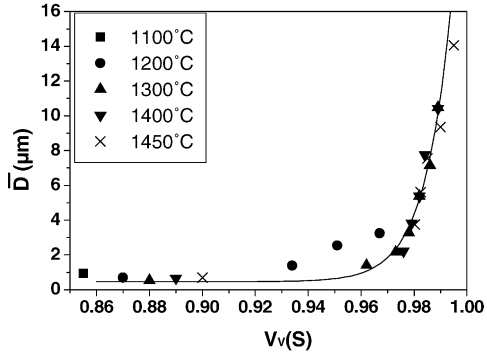

Fig. 12. Sintering trajectory: evolution of the mean grain size, $\bar{D}$, as a function of the volume fraction of ceria V_V(S).

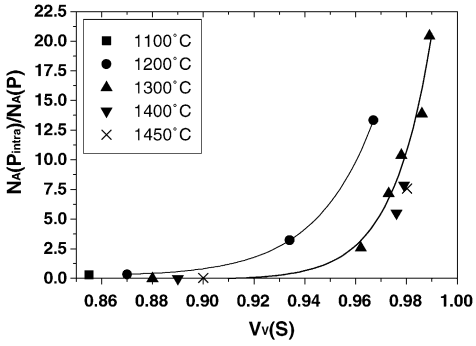

Fig. 13. Variation of intra-granular porosity, $N_A(P_{intra})/N_A(P)$, as a function of volume fraction of ceria, $V_V(S)$.

lower than 97% of the theoretical density, for temperatures higher than 1300 °C. Then, for larger densities, grain growth becomes predominant. At 1200 °C, grain growth begins at a lower density, so earlier in the densification process. At low temperature, the TiO_2 dopant seems to be less efficient as a grain growth inhibitor than at temperature higher than 1300 °C. At 1200 °C, $CeTi_2O_6$ is not formed and only TiO_2 inclusions can act to reduce the grain boundary mobility. At 1300 °C, $CeTi_2O_6$ is formed and $CeTi_2O_6$ inclusions seem to have a higher influence on the decrease of the grain boundary mobility. The lower volume fraction of TiO_2 (0.17% with respect to CeO_2) than of $CeTi_2O_6$ (calculated values of 0.25%, considering that all TiO_2 reacts with CeO_2 to form $CeTi_2O_6$) could explain its lower impact on grain growth.

At 1300 °C, the melting point of $CeTi_2O_6$ being close to that of the sintering temperature, the densification rate could be accelerated by the presence of a liquid phase, which can form locally. This phenomenon was already observed in the case of CeO_2 doped by TiO_2,[13] and for several ceramic systems, as for example CaO/Al_2O_3.[35] At 1400 and 1450 °C, the presence of a liquid phase at grain boundaries is expected to increase the matter transport by a mechanism of dissolution–diffusion–reprecipitation (liquid phase sintering).

The evolution of the grain size gradually governs the change of the porosity in intra-granular positions. Indeed, the evolution of porosity in intra-granular positions as a function of the volume fraction (Fig. 13) seems to follow the same evolution as the grain size (Fig. 12). In spite of a relatively low porosity content, the more grain growth occurs, the more the ratio of pores in intragranular positions, $N_A(P_{intra})/N_A(P)$, increases. This is due to the difference between the mobility of the grain boundaries and the pores.

4. Conclusion

This paper demonstrated the importance of automatic image analysis in making it possible to access the change in morphological parameters during sintering, such as the specific surface areas, the integral of mean curvature per unit volume, or the contiguity, as a function of the volume fraction of solid, the temperature or the time. Another advantage of this method is to reveal about the extent of homogeneity of the material from variograms (of the number of grains or of the volume fraction of pores, for our investigation).

CeO_2 ceramic was chosen for this work, for which specific image treatments and segmentation techniques were developed, depending on the densification state. A very good homogeneity was shown in the bulk material.

The accurate investigation of the sintering trajectory and of the change in the stereological parameters indicates that grain growth in CeO_2 is more important at 1200 °C for a lower densification state than at 1300 °C. This is probably due to the presence of the $CeTi_2O_6$ secondary phase, which forms at 1270 °C. The obtained activation energy is ≈400 kJ mol^{-1}, a value of the same order of magnitude as that of Y_2O_3.[25]

The correct knowledge of the grain size distributions of ceria is very important for sintering investigations, not only to determine the densification and grain growth mechanisms, but also to model the ceria microstructures.[14,36] We have found evidence for a volume diffusion mechanism of the slowest species, with dopant segregation at the CeO_2 grain boundaries, the TiO_2 dopant appears to control the CeO_2 grain boundary migration in limiting grain growth. At 1300 °C, the presence of a liquid phase based on $CeTi_2O_6$ can increase the matter transport by a dissolution–diffusion–reprecipitation mechanism.

From all these results, the simulation of these different microstructures has been undertaken with success, with good agreements having been obtained for measurements on simulated and experimental microstructures.[14,36] These simulations are based on probabilistic tools and appear to be promising methods to describe the 3D microstructures of many types of materials including powders, ceramics, concrete, and metals.[36–39]

Acknowledgments

This work was performed at LERMAT (URA CNRS 1317, ISMRA, Caen, France) in the frame of the CRITIC (Comité Régional de l'Image et des Technologies de l'Information et de la Communication) Pole, that we thank. It has been financially supported by two contracts: "Granulométrie et modélisation de céramiques", 1999 nb 99.12, and "Modélisation et logiciel de granulométrie de matériaux granulaires", 2001 nb 01.285. The authors, and more specially X. Arnould, are grateful to ADCIS, Caen, France, for its financial support and discussions.

Appendix A. Stereological method to measure $S_V(S/P_{intra})$, $S_V(S/P_{inter})$ and $S_V(S/S)$

A.1. Manual stereological analysis method

On the microphotography (Fig. A), grains and pores are crossing by horizontal lines. One line corresponds to a line

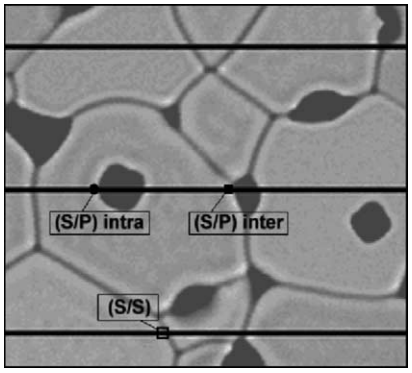

Fig. A. Illustration of stereological method to measure the S_V parameters.

of pixels on the digital image. The points which correspond to the following transitions are marked on these lines:

- grains boundary (S/S),
- solid-pore (S/P_{intra}),
- solid-pore (S/P_{inter}).

The number of these transitions by unit of length of line allows to calculate the following parameters: $N_L(S/S)$, $N_L(S/P_{intra})$ and $N_L(S/P_{inter})$.

The stereological relationship ($S_V(X/Y) = 4N_L(X/Y)$) makes it possible to calculate the corresponding specific surface area per unit volume.

A.2. Automatic stereological analysis method

Three binary images from image processing are used:

- the image of grains boundaries,
- the image of pores in position intra,
- the image of pores in position inter.

The number of transitions of 1–0 type allows to measure the previous parameters.

References

1. Herring, C., Diffusional viscosity of a polycristalline solid. *J. Appl. Phys.*, 1950, **21**, 437–445.
2. Coble, R. L., Sintering crystalline solids. I: Intermediate and final diffusion models. *J. Appl. Phys.*, 1961, **32**(5), 787–792.
3. Coble, R. L., Sintering crystalline solids. II: Experimental test of diffusion model in powder compacts. *J. Appl. Phys.*, 1961, **32**(5), 787–792.
4. Brook, R. J., Pore grain boundary interaction and grain growth. *J. Am. Ceram. Soc.*, 1969, **52**, 56–57.
5. Brook, R. J., Pores and grain growth kinetics. *J. Am. Ceram. Soc.*, 1969, **52**, 339–340.
6. Kingery, W. D. and François, B., Sintering crystalline oxides. I: Interactions between grain boundaries and pores. In *Sintering and Related Phenomena*, ed. G. C. Kuczynski, N. A. Hooton and G. F. Gibbon. Gordon and Breach, New-York, 1967, pp. 471–498.
7. DeHoff, R. T., *Quantitative Microscopy*. McGraw Hill, New York, 1968.
8. Chermant, J. L., Coster, M. and Jernot, J. P., Application of quantitative metallography in sintering investigation. V: Contribution of image analysis to solid state sintering investigation. *Pract. Met.*, 1984, **21**, 567–580.
9. Chermant, J. L., Coster, M. and Jernot, J. P., Morphololological analysis of sintering. *J. Microsc.*, 1981, **121**, 89–98.
10. Serra, J., *Image Analysis and Mathematical Morphology*. Academic Press, London, 1982.
11. Coster, M. and Chermant, J. L., *Précis d'analyse d'images. Les éditions du CNRS* (*2ème éd.*). Les Presses du CNRS, Paris, 1989.
12. Jernot, J. P., *Analyze morphologique et modélisation du frittage et des matériaux fragiles*. Thèse de Doctorat ès Sciences Physiques, University of Caen, France, 1982.
13. Argoita, A., *Elaboration et propriétés de céramiques à base d'oxyde de cerium*. Thèse de Doctorat of the University of Limoges, France, 1986.
14. Arnould, X., *Granulométrie et modélisation de céramiques*. Thèse de Doctorat of the University of Caen, France, 2002.
15. Fauvarque, J. F., Les piles à combustibles et leurs applications. *Ann. Chim. Sci. Mater.*, 2001, **26**(4), 1–8.
16. Suzuki, T., Kosacki, I., Anderson, H. U. and Colomban, P., Electrical conductivity and lattice defects in nanocrystalline cerium oxide thin films. *J. Am. Ceram. Soc.*, 2001, **84**(9), 2007–2014.
17. Inada, H. and Tagawa, H., Ceria-based solid electrolytes. *Solid State Ionics*, 1996, **83**, 1–16.
18. Matze, H. j., Rondinella, V. V. and Wiss, T., Materials research on inert matrices: a screening study. *J. Nucl. Mater.*, 1999, **274**(1/2), 47–53.
19. Kosacki, I., Suzuki, T. and Anderson, H. U., The growth and optical properties of ZrO_2:Y and CeO_2 nanocristallyne thin films. In *Innovative Processing/Synthesis: Ceramics, Glasses, Composites III*. *Ceram. Trans*., 2000, **108**, 275–284.
20. Arnould, X., Coster, M., Chermant, J. L., Chermant, L., Chartier, T. and El-Moataz, A., Segmentation and grain size of ceramics. In *8th European Congress for Stereology and Image Analysis, 8 ECSIA*, Bordeaux, France, September 4–7, 2001. CD ROM ed. Anguy, Y., Riss, J., and *Image Anal. Stereol.*, 2001, **20**, 131–135.
21. Arnould, X., Coster, M., Chermant, J. L., Chermant, L., Chartier, T., Ceramography and segmentation of polycristalline ceramics: application to grain size analysis by automatic method. In *7th Congress of the European Ceramic Society, 7 ECRS*. Brugge, Belgium, September 9–13, 2001. *Trans. Tech. Pub., Key Eng. Mater.*, 2002, **206**–**213**, 685–690.
22. Matheron, G., *Les variables régionalisées et leur estimation: une application de la théorie des fonctions aléatoires aux sciences de la nature*. Masson, Paris, 1965.
23. DeHoff, R. T., Scale factor coarsening. *Metallography*, 1984, **17**, 203–208.
24. Coble, R. L. and Gupta, T. K., Intermediate stage sintering. In *Sintering and Related Phenomena*, ed. G. C. Kuczynski. Gordon and Breach, Science Publishers, New York, 1967, pp. 423–443.
25. Gasgnier, G., *Densification de l'oxyde d'yttrium*. Thèse de Doctorat of the University of Limoges, 1991.
26. Chen, P. L. and Chen, I. W., Grain growth in CeO_2: dopant effects, defect mechanism, and solute drag. *J. Am. Ceram. Soc.*, 1996, **79**(7), 1793–1800.
27. Zhang, T., Hing, P., Huang, H. and Kilner, J., Sintering study on commercial CeO_2 powder with small amount of MnO_2 doping. *Mater. Lett.*, 2002, **57**, 507–512.
28. Zhang, T. S., Ma, J., Kong, L. B., Zeng, Z. Q., Hing, P. and Kilner, J. A., Final-stage sintering behavior of Fe-doped CeO_2. *Mater. Sci. Eng. B*, 2003, **103**, 177–183.
29. Zhang, T., Hing, P., Huang, H. and Kilner, J., Sintering and grain growth of CoO-doped CeO_2 ceramics. *J. Eur. Ceram. Soc.*, 2002, **22**, 27–34.

30. Li, J.-G., Ikegami, T. and Mori, T., Low temperature processing of dense samarium-doped CeO_2 ceramics: sintering and grain growth behaviors. *Acta Mater.*, 2004, **52**, 2221–2228.
31. Brook, R. J., Controlled grain growth. In *Treatise on Materials Science and Technology, Ceramic Fabrication Processes (Vol 9)*, ed. F. F. Y. Wang. Academic Press, New-York, 1976, pp. 331–364.
32. Guka, J. P. and Kolar, D., Subsolidus equilibria in the system $BaO–CeO_2–TiO_2$. *J. Am. Ceram. Soc.*, 1973, **56**(1), 5–6.
33. Michels, A., Krill, C. E., Ehrhardt, H., Birringer, R. and Wu, D. T., Modeling the influence of grain-size-dependent solute drags on the kinetics of grain growth in nanocrystalline materials. *Acta Mater.*, 1999, **47**(7), 2143–2152.
34. Chen, P. L. and Chen, I. W., The role of defect interaction in boundary mobility and cation diffusivity of CeO_2. *J. Am. Ceram. Soc.*, 1994, **77**, 2289–2297.
35. Wu, S. J., De Jonghe, L. C. and Rahaman, R. N., Subeutectic densification and second-phase formation in Al_2O_3–CaO. *J. Am. Ceram. Soc.*, 1985, **68**(7), 385–388.
36. Coster, M., Arnould, X., Chermant, J. L., El Moataz, A. and Chartier, T., Microstructural model for sintered ceramics: the cerine. *Imag. Anal. Stereol.*, in press.
37. Coster, M. and Chermant, J. L., On a way to material models for ceramics. *J. Eur. Ceram. Soc.*, 2002, **22**, 1191–1203.
38. Dequiedt, A. S., Coster, M., Chermant, J. L. and Jeulin, D., Towards a model of concrete mesostructure. *Cem. Concr. Comp.*, 2001, **23**, 289–297.
39. Decker, L. and Jeulin, D., Simulation 3D de matériaux aléatoires polycristallins. *Rev. Meter. CIT Sci. Génie. Mater.*, 2000, **97**, 271–275.